

Band gap renormalization, carrier mobilities, and the electron-phonon self-energy in crystalline naphthalene

Florian Brown-Altwater^{1,2,*}, Gabriel Antonius^{3,4}, Tonatiuh Rangel^{2,4}, Matteo Giantomassi⁵, Claudia Draxl⁶,
Xavier Gonze^{5,7}, Steven G. Louie^{4,8}, and Jeffrey B. Neaton^{2,4,9,†}

¹Department of Chemistry, University of California, Berkeley, California 94720, USA

²Molecular Foundry, Lawrence Berkeley National Laboratory, Berkeley, California 94720, USA

³Département de Chimie, Biochimie et Physique, Institut de Recherche sur l'Hydrogène, Université du Québec à Trois-Rivières, C.P. 500, Trois-Rivières, Canada G9A 5H7

⁴Department of Physics, University of California, Berkeley, California 94720, USA

⁵Institute of Condensed Matter and Nanosciences, Université Catholique de Louvain, 1348 Louvain-la-Neuve, Belgium

⁶Institut für Physik, Humboldt Universität Berlin, 12489 Berlin, Germany

⁷Skolkovo Institute of Science and Technology, 121205 Moscow, Russia

⁸Materials Sciences Division, Lawrence Berkeley National Laboratory, Berkeley, California 94720, USA

⁹Kavli Energy NanoSciences Institute at Berkeley, California 94720, USA



(Received 17 December 2019; accepted 27 February 2020; published 2 April 2020)

Organic molecular crystals are expected to feature appreciable electron-phonon interactions that influence their electronic properties at zero and finite temperature. In this work, we report first-principles calculations and an analysis of the electron-phonon self-energy in naphthalene crystals. We compute the zero-point renormalization and temperature dependence of the fundamental band gap, and the resulting scattering lifetimes of electronic states near the valence- and conduction-band edges employing density functional theory. Further, our calculated phonon renormalization of the GW-corrected quasiparticle band structure predicts a fundamental band gap of 5 eV for naphthalene at room temperature, in good agreement with experiments. From our calculated phonon-induced electron lifetimes, we obtain the temperature-dependent mobilities of electrons and holes in good agreement with experimental measurements at room temperature. Finally, we show that an approximate energy self-consistent computational scheme for the electron-phonon self-energy leads to the prediction of strong satellite bands in the electronic band structure. We find that a single calculation of the self-energy can reproduce the self-consistent results of the band gap renormalization and electrical mobilities for naphthalene, provided that the on-the-mass-shell approximation is used, i.e., if the self-energy is evaluated at the bare eigenvalues.

DOI: [10.1103/PhysRevB.101.165102](https://doi.org/10.1103/PhysRevB.101.165102)

Molecular crystals, periodic arrays of molecules bound by noncovalent interactions, can nonetheless feature relatively high charge carrier mobilities [1–4]. The acene family of molecular crystals are of particular interest, having high crystalline purity, making them attractive for fundamental studies and various optoelectronic applications [5–8]. In acenes, each monomer consists of a rigid unit of fused benzene rings. These monomers crystallize in a herringbone structure (Fig. 1). Naphthalene, the second smallest of the acene family, provides a popular testbed for electronic structure calculations and experiments, with results that can often be extrapolated to its larger siblings [9].

Electron-phonon coupling (EPC) has long been understood to be important in determining the electronic and transport properties of these materials [10–12]. Along with contributions from thermal lattice expansion, the EPC is responsible for the temperature-dependent renormalization of the band structure. Electron-phonon scattering and decay channels also

result in finite lifetimes for electronic states and limit charge carrier mobilities. The finite lifetimes result in a broadening of the electronic bands that can be observed with photoemission spectroscopy, for example [13,14].

The vast majority of prior theoretical studies of temperature effects in organic crystals arising from EPC focus on lifetimes and mobilities of charge carriers [4,12,15–27]. Prior *ab initio* studies that explicitly calculate the renormalization of band gaps are usually limited to few-atom systems [28–33] or small molecules [34]. One study that calculated both the broadening and renormalization of the band gap of pentacene crystals used a tight-binding model parametrized by many-body perturbation theory (MBPT) calculations [35], reporting unusual quasidiscontinuities in the band structure caused by EPC that have been corroborated by experimental results, showing “kinks” in the electronic dispersion [35,36]. In another study, Vukmirović *et al.* [37] evaluated the EPC matrix elements for two pairs of bands in naphthalene using first-principles methods. They reported weak EPC, strengthening the argument for bandlike charge carrier transport. Lee *et al.* [25] use a fully *ab initio* approach to calculate the temperature-dependent hole mobility.

*altwater@berkeley.edu

†jbneaton@berkeley.edu

In this work, we compute from first principles the temperature dependence of the band structure and the electron and hole transport properties of naphthalene crystals. We use density functional theory and the dynamical Allen-Heine-Cardona theory to compute both the real and imaginary contributions to the electron-phonon self-energy. With this quantity, we predict the temperature renormalization of the band gap, and we obtain the hole and electron mobilities within the relaxation-time approximation. We discuss the details of the calculated frequency-dependent electron-phonon self-energy of the electron or hole, and identify features that should apply to acene and other molecular solids, such as the approximate independence of the self-energy on the electron wave vector \mathbf{k} . We find that in naphthalene, the band dispersion, phonon frequencies, and the renormalization energies are of the same order of magnitude, challenging the validity of perturbation theory in this system. We address this issue by exploring a self-consistent computational scheme for the electron-phonon self-energy, and we show that a single calculation of the self-energy can reproduce self-consistent results of the band gap renormalization and charge carrier mobilities, provided that the on-the-mass-shell approximation is used.

I. THEORY AND METHODS

A. Theoretical framework

The starting point for our calculations is density functional theory (DFT), which provides Kohn-Sham orbital wave functions $\psi_{n\mathbf{k}}$ and orbital energies $\epsilon_{n\mathbf{k}}^0$, where n is the band index and \mathbf{k} is the wave vector. We rely on density functional perturbation theory (DFPT) to compute the phonon coupling potential, and we incorporate the electron-phonon interactions via many-body perturbation theory, specifically a low-order diagrammatic expansion of the electron-phonon self-energy [38–40].

To obtain the electron-phonon self-energy, we follow the approach described in [31,41]. To lowest order in perturbation theory, the electron-phonon self-energy $\Sigma_{n\mathbf{k}}^{\text{ep}}$ can be divided into two terms, namely the Fan and Debye-Waller (DW) terms

$$\Sigma_{n\mathbf{k}}^{\text{ep}}(\omega, T) = \Sigma_{n\mathbf{k}}^{\text{Fan}}(\omega, T) + \Sigma_{n\mathbf{k}}^{\text{DW}}(T). \quad (1)$$

We briefly summarize each term. The frequency-dependent Fan term is given as

$$\begin{aligned} \Sigma_{n\mathbf{k}}^{\text{Fan}}(\omega, T) = & \sum_{\nu\mathbf{q}} \frac{1}{2\omega_{\nu\mathbf{q}}} \sum_m |g_{nm\nu}(\mathbf{k}, \mathbf{q})|^2 \\ & \times \left[\frac{N_{\nu\mathbf{q}}(T) + f_{m\mathbf{k}+\mathbf{q}}(T)}{\omega - \epsilon_{m\mathbf{k}+\mathbf{q}}^0 + \omega_{\nu\mathbf{q}} + i\eta} \right. \\ & \left. + \frac{N_{\nu\mathbf{q}}(T) + 1 - f_{m\mathbf{k}+\mathbf{q}}(T)}{\omega - \epsilon_{m\mathbf{k}+\mathbf{q}}^0 - \omega_{\nu\mathbf{q}} + i\eta} \right]. \end{aligned} \quad (2)$$

In Eq. (2), the phonon modes are specified by indices ν , wave vector \mathbf{q} , and energies $\omega_{\nu\mathbf{q}}$. Phonons couple electrons in state $n\mathbf{k}$ with state $m\mathbf{k}+\mathbf{q}$ through the first derivative of the electron crystal potential $V_{\nu\mathbf{q}}^{(1)}$ associated with the respective phonon's atomic displacement pattern. The electron-phonon matrix elements $g_{nm\nu}(\mathbf{k}, \mathbf{q}) = \langle \psi_{n\mathbf{k}} | V_{\nu\mathbf{q}}^{(1)} | \psi_{m\mathbf{k}+\mathbf{q}} \rangle$ determine the coupling strength between the electronic states and the phonons. The

temperature dependence of the Fan term arises from the phonon (N) and electron (f) occupation factors. We can see that even at zero temperature, the self-energy has a finite value. The denominators give rise to poles at $\omega = \epsilon^0 \pm \omega_{\nu\mathbf{q}}$, which are rendered smooth with the parameter η ; η , in principle, is real, infinitesimal, and has the same sign as ω in Eq. (2), which yields the time-ordered self-energy, in contrast to the retarded self-energy [40]. In practice, we use a value of 0.025 eV to account for the finite \mathbf{q} -grid sampling. Details of the convergence of the self-energy with respect to \mathbf{q} -grid and η can be found in the Supplemental Material [42].

The frequency-independent Debye-Waller term

$$\Sigma_{n\mathbf{k}}^{\text{DW}}(T) = \sum_{\nu\mathbf{q}} \frac{1}{2\omega_{\nu\mathbf{q}}} \langle n\mathbf{k} | V_{\nu\mathbf{q},\nu\mathbf{q}}^{(2)} | n\mathbf{k} \rangle [2N_{\nu\mathbf{q}}(T) + 1] \quad (3)$$

makes up the second part of the electron-phonon self-energy. The DW term depends on the second derivative of the potential $V_{\nu\mathbf{q},\nu\mathbf{q}}^{(2)}$, which is somewhat more arduous to calculate. We use the rigid-ion approximation, which allows us to write Eq. (3) in terms of the first derivative [38,43,44]. In this way, we can obtain all values from DFT and DFPT calculations.

There are two main challenges in calculating the self-energy efficiently. The first challenge is that \mathbf{q} -space has to be sampled more densely compared to a typical phonon band structure calculation, which rapidly becomes the main bottleneck for large systems. In this work, we interpolate the phonon coupling potential in real space, following prior work [45–48]. It is standard practice to interpolate the phonon frequencies of a regular \mathbf{q} -grid onto arbitrary \mathbf{q} -points by means of a Fourier transform of the dynamical matrices to real space, and back to reciprocal space. Applying the same principle here, we calculate the potential derivative with DFPT on a coarse \mathbf{q} -point grid and interpolate to a finer grid via Fourier transform. We define the long-range component of the phonon potential of atom κ along the Cartesian direction j as

$$V_{\kappa j}^L(\mathbf{q}, \mathbf{r}) = i \frac{4\pi}{\Omega} \sum_{\mathbf{G} \neq -\mathbf{q}} \frac{e^{i(\mathbf{q}+\mathbf{G}) \cdot (\mathbf{r}-\mathbf{r}_\kappa)} (\mathbf{q}+\mathbf{G})_{j'} \cdot \mathbf{Z}_{\kappa,j'j}^*}{(\mathbf{q}+\mathbf{G}) \cdot \epsilon^\infty \cdot (\mathbf{q}+\mathbf{G})}, \quad (4)$$

where ϵ^∞ is the static dielectric matrix without the lattice contribution to the screening, and $\mathbf{Z}_{\kappa,j'j}^*$ is the Born effective charge tensor. These quantities are computed from DFPT by including the response of the system to a macroscopic electric field. The long-ranged component of the phonon potential represents the dipole potential created by displacing the Born effective charges of each atom, and becomes the dominant contribution to the potential in the limit $\mathbf{q} \rightarrow \mathbf{0}$. Next, we perform a Fourier transform of the short-range component of the phonon coupling potential, starting from the coarse \mathbf{q} -point grid,

$$W_{\kappa j}(\mathbf{r} - \mathbf{R}_l) = \sum_{\mathbf{q}} e^{i\mathbf{q} \cdot \mathbf{R}_l} [V_{\kappa j}^{(1)}(\mathbf{q}, \mathbf{r}) - V_{\kappa j}^L(\mathbf{q}, \mathbf{r})], \quad (5)$$

where $W_{\kappa j}(\mathbf{r} - \mathbf{R}_l)$ represents the short-range component of the perturbative potential associated with the displacement of atom κ in the unit cell l along the Cartesian direction j , and \mathbf{r} is defined within the first unit cell ($\mathbf{R}_0 = \mathbf{0}$). The interpolated

phonon potential for an arbitrary point $\tilde{\mathbf{q}}$ is then

$$V_{\kappa j}^{(1)}(\tilde{\mathbf{q}}, \mathbf{r}) \approx \sum_l W_{\kappa j}(\mathbf{r} - \mathbf{R}_l) e^{-i\tilde{\mathbf{q}} \cdot \mathbf{R}_l} + V_{\kappa j}^L(\tilde{\mathbf{q}}, \mathbf{r}). \quad (6)$$

This interpolation scheme reproduces the electron-phonon coupling matrix elements with accuracy better than 1%, as shown in the Supplemental Material [42]. It achieves the same goal as the Wannier interpolation used in other works [48–50], but avoids the computation of Wannier functions altogether.

The second challenge in the computation of the electron-phonon self-energy lies in the sum over electronic states m in Eq. (2), which can converge slowly with the number of bands. We evaluate this sum explicitly using all valence bands and conduction bands up to 5 eV above the last electronic state for which the self-energy is computed. Above this cutoff, the sum over infinite bands is replaced by a Sternheimer equation, and their contribution to the self-energy is treated statically, an approximation that has been shown to be effective in prior work [41,44]. Furthermore, this contribution is evaluated on the coarse \mathbf{q} -grid, since the denominator of the self-energy in Eq. (2) is never small for these bands, and is thus a smooth function of \mathbf{q} .

B. Computational details

DFT calculations are performed with the ABINIT code [47,51,52] using Fritz-Haber-Institut norm-conserving pseudopotentials [53], and setting the plane wave kinetic energy cutoff to 45 Ha. We use the Perdew-Burke-Ernzerhof (PBE) functional in combination with the Grimme-D3 correction [54,55] to account for London dispersion forces. To obtain the electronic ground state density, we sample the Brillouin zone on a Γ -centered \mathbf{k} -grid of $2 \times 4 \times 2$. All electronic energies in this work are given relative to the valence-band maximum.

The phonons and associated potential derivatives are calculated with DFPT, including the treatment of dispersion forces [56–59]. A coarse Γ -centered $4 \times 6 \times 4$ \mathbf{q} -grid gives well-converged phonon frequencies and displacements after interpolation of the dynamical matrix, as shown in our previous work [60]. In the present work, we start from an even finer $6 \times 8 \times 6$ grid, and we interpolate not only phonon frequencies and displacements, but also the phonon potentials and self-energy onto a $12 \times 14 \times 12$ \mathbf{q} -grid, which converges the renormalization and broadening values within a few meV (see the Supplemental Material [42] for convergence studies).

C. Lattice parameters

Naphthalene crystallizes in the $P2_1/a$ space group, forming a herringbone structure with two molecules per unit cell (Fig. 1) that are held together by noncovalent interactions. As discussed in previous work [61], relaxing lattice parameters and atomic coordinates with van der Waals corrected functionals or pairwise dispersion corrections results in excellent agreement with low-temperature experiments. The relaxed unit-cell volume of naphthalene obtained with PBE-D3 is within 0.4% of the experimental value measured at 5 K.¹

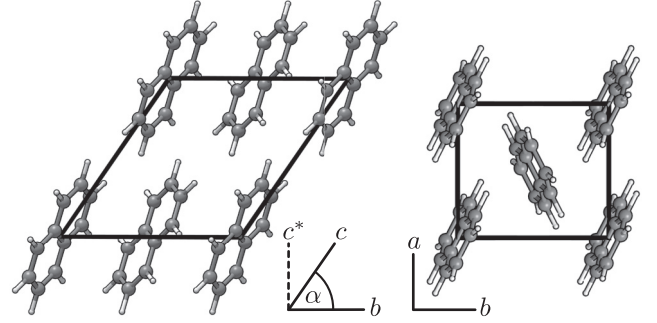


FIG. 1. Naphthalene is the smallest acene that crystallizes in a herringbone structure. There are two molecules in the monoclinic unit cell, each situated at inversion centers.

We use this relaxed unit cell for most of our calculations, and we refer to it by its computed volume, Ω_{DFT} . To simulate thermal lattice expansion, we use fixed experimental lattice parameters obtained at 295 K,¹ and we relax the internal atomic coordinates using PBE-D3. The volume of this room-temperature structure is about 6% larger than that of the low-temperature structure. The main expansion occurs in the ab plane, and through a decreased tilt of the monoclinic cell (see the Supplemental Material for all unit-cell parameters [42]). Any calculations that use this experimental lattice are labeled by this larger volume, $\Omega_{295\text{K}}$.

II. RESULTS AND DISCUSSION

A. Electronic and phonon band structures

The electronic band structure of naphthalene is characteristic for a small molecule crystal [61]: it possesses a sizable band gap combined with flat, well-separated groups or complexes of bands (Fig. 2). DFT yields an indirect gap of 3.01 eV between the valence-band maximum (VBM) at A and the conduction-band minimum (CBM) at Γ . The weak intermolecular interactions lead to small bandwidths for the complexes less than 0.4 eV. Furthermore, because naphthalene has two molecules per unit cell, the electronic bands double up in so-called Davydov pairs [64,65]. In the vicinity of the band gap, these Davydov pairs are separated from each other by about 0.4 eV. This separation drastically reduces mixing of states from different Davydov pairs. The wave functions of solid naphthalene at the band edges therefore vary little throughout the Brillouin zone, and closely resemble linear combinations of gas-phase-like molecular orbitals. Dispersion and interband interactions are higher for bands just below -2 eV as the spacing between electronic levels decreases, and for bands above 4.5 eV as the wave functions become more delocalized.

For the phonon frequencies, we obtain excellent agreement with experiments across the Brillouin zone using PBE-D3 (see the Supplemental Material [42] for the full phonon band structure in comparison with experimental

¹The experimental crystal structures used in this work are available at the Cambridge Structural Database [62]. The identifiers for the

structures measured at 5 and 295 K are NAPHTA31 and NAPHTA36, respectively, and published in association with [63].

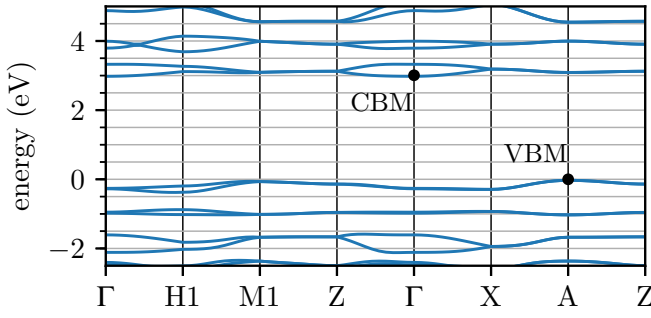


FIG. 2. Electronic band structure of naphthalene calculated with DFT. The locations of the conduction-band minimum (CBM) and valence-band maximum (VBM) are indicated with black dots.

measurements from Refs. [66,67]), similar to our previous results with the vdW-DF-cx functional [60]. Since we analyzed the vibrational properties of naphthalene in depth in Ref. [60], we give only a brief overview of the main features here. In naphthalene, intermolecular modes (<20 meV) can be clearly distinguished from intramolecular modes (20–400 meV). Intermolecular modes are translational and librational modes of rigid molecules, while for intramolecular modes, the phonon displacement vectors resemble linear combinations of gas phase vibrations.

We emphasize that, despite the clear separation between inter- and intramolecular modes, we treat all phonon modes on the same footing in our work. While hopping transport models often use the rigid molecule approximation [68–70], it has been shown that the mixed inter- and intramolecular low-frequency modes can have large EPC contributions, especially for larger molecules like rubrene [71].

Upon thermal lattice expansion, the spacing between molecules becomes larger. The lowered interaction leads to softening of the intermolecular modes, decreasing the lowest frequencies by up to 40%. In contrast, intramolecular frequencies, which depend on the covalent interatomic forces, are found to change very little, as shown in the Supplemental Material [42].

B. Temperature-dependent renormalization of the band structure

We obtain the temperature-dependent electronic band structure of naphthalene from the real part of the electron-phonon self-energy using the on-the-mass-shell approximation [72]

$$\varepsilon_{nk}(T) = \varepsilon_{nk}^0 + \text{Re}[\Sigma_{nk}^{\text{ep}}(\varepsilon_{nk}^0, T)], \quad (7)$$

where ε_{nk}^0 is the bare DFT eigenvalue with band index n and wave vector \mathbf{k} , and ε_{nk} is the renormalized energy.

The temperature dependence of the VBM, CBM, and indirect band gap at fixed lattice parameters and neglecting thermal expansion is shown in Fig. 3. The zero-point renormalization (ZPR) of the DFT band gap is calculated to be -0.23 eV, with nearly equal contributions from a decrease of the CBM (-0.12 eV) and an increase of the VBM energies ($+0.11$ eV). This large correction reduces the DFT-PBE gap from 3.01 to 2.78 eV.

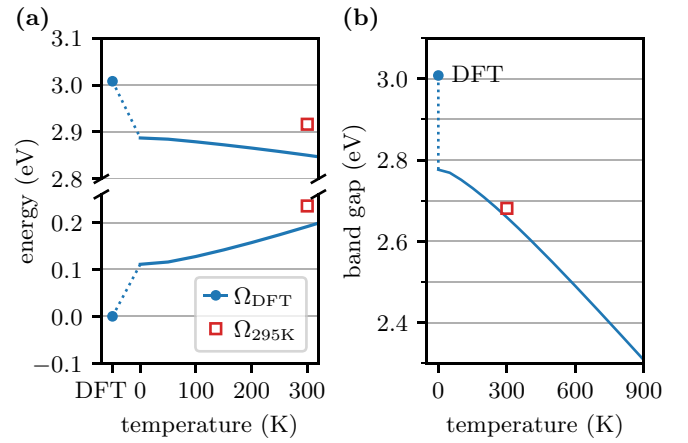


FIG. 3. (a) Renormalization and temperature dependence of the band edge states at Γ and A , with Ω_{DFT} . The dotted lines indicate the ZPR, connecting the bare eigenvalues calculated with PBD-D3 (circles) with the renormalized energies at 0 K. The renormalized energies for $\Omega_{295\text{K}}$ (squares) at 300 K are plotted for comparison. (b) ZPR (dotted) and temperature dependence (solid) of the indirect band gap of naphthalene for Ω_{DFT} . The red square shows the renormalization at 300 K using $\Omega_{295\text{K}}$.

At 300 K, the band gap at unit-cell volume Ω_{DFT} is predicted to be reduced by an additional -0.12 eV. The rate of change of the gap at this temperature is 0.05 eV/100 K, and increases only slightly to the linear limit of 0.064 eV/100 K at temperatures beyond 500 K.

The DFT gap for the experimental room-temperature structure at the enlarged volume $\Omega_{295\text{K}}$ is 3.12 eV, an increase of 0.11 eV compared to Ω_{DFT} . The renormalization calculated at 300 K (-0.44 eV) brings it down to 2.68 eV. We observe that the two contributions to the renormalization we compute—the lattice expansion and the zero-temperature contribution from the electron-phonon interaction—are not independent, additive terms. The EPC shows non-negligible volume dependence, with the renormalization increasing by 26% from -0.35 eV at Ω_{DFT} to -0.44 eV at $\Omega_{295\text{K}}$. This can be explained by a narrowing of the electronic bands upon lattice expansion and hence an increase in the electronic DOS. The increased DOS near and at the band edges leads to more scattering channels on the scale of the phonon energies, and thus an overall larger self-energy. Altogether, the volume expansion of $\Omega_{295\text{K}}$ leads to two contributions to the renormalization of opposite signs, resulting in a band gap at 300 K that is only 70 meV smaller than the value at 0 K.

For a more detailed analysis of the ZPR and temperature dependence, we examine the individual phonon contributions to the renormalization. Reorganizing Eq. (1), we can write

$$\Sigma_{nk}^{\text{ep}}(\omega) = \sum_{\nu\mathbf{q}} [\Sigma_{nk,\nu\mathbf{q}}^{\text{Fan}}(\omega) + \Sigma_{nk,\nu\mathbf{q}}^{\text{DW}}] = \sum_{\nu\mathbf{q}} \Sigma_{nk,\nu\mathbf{q}}^{\text{ep}}(\omega) \quad (8)$$

to obtain the contribution from each phonon. For this analysis, we calculate the self-energy on a \mathbf{q} -grid of $6 \times 8 \times 6$, since this phonon decomposition does not hold for our interpolation scheme with two \mathbf{q} -grids.

In Fig. 4 we plot the real part of each $\Sigma_{nk,\nu\mathbf{q}}^{\text{ep}}(\varepsilon_{nk}^0)$ at 0 K—i.e., each phonon’s contribution to the ZPR. To account for

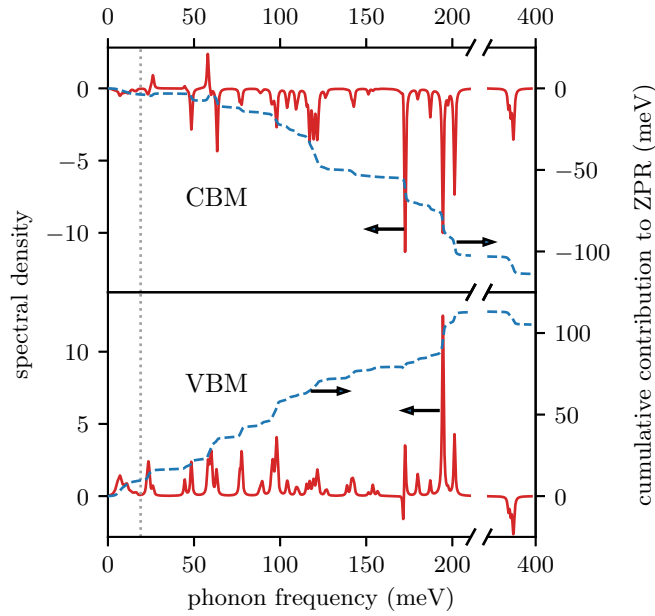


FIG. 4. Individual contributions of the phonon modes to the renormalization of the CBM and VBM plotted against frequency, with a Lorentzian smearing of 1 meV (red solid line, left axis). The gray dotted line at 19 meV indicates the separation of inter- from intramolecular modes. The blue dashed line (right axis) shows the cumulative integral of the individual contributions.

a finite sampling of reciprocal space, we used a Lorentzian broadening of 1 meV. The intramolecular phonon modes around 190 meV are found to have the largest individual contributions, in agreement with previous studies [25,37]. Overall, however, the contribution as a function of phonon frequency is distributed relatively equally over the frequency range, especially for the VBM, as can be seen from the integral of the spectral density [blue line in Fig. 4(a)]. The intermolecular modes situated below 19 meV (gray dashed line in Fig. 4) contribute comparatively little to the ZPR. Only these weakly coupling intermolecular and a few soft intramolecular modes are populated at ambient temperatures, and contribute to the further reduction of the gap at finite temperatures.

A more quantitative description of the fundamental band gap can be achieved by correcting the DFT band gap with many-body perturbation theory within the *GW* approximation for the self-energy due to electron-electron interaction, then adding the EPC corrections to account for the electron-phonon interaction. Our previous work shows that the *GW* method increases the indirect DFT band gap of naphthalene by about 2.3 eV [61], thus bringing the band gap of the expanded room-temperature structure to 5.4 eV. Adding the electron-phonon coupling renormalization computed at 300 K, we obtain a fundamental gap of 5.0 eV, in excellent agreement with the experimental room temperature value of 5 eV [73].

The electron-electron correlation itself affects the EPC, as reported in prior work, and efforts have been put toward developing methods to capture and quantify this effect [33,34,74–76]. Considering the similarity of the magnitudes of electronic bandwidth, phonon, and electron-phonon coupling energies in

TABLE I. Calculated mobilities in comparison with experimental values. We interpolated the experimental results reported in Ref. [80] to 50 and 300 K, and we compare them to calculations using the relaxed (Ω_{DFT}) and experimental room-temperature volume ($\Omega_{295\text{K}}$), respectively. Mobility values are given along crystal vectors a and b , as well as c^* , defined as the vector perpendicular to the ab plane. All values in $\text{cm}^2/\text{V s}$.

	Hole			Electron		
	μ_a^h	μ_b^h	$\mu_{c^*}^h$	μ_a^e	μ_b^e	$\mu_{c^*}^e$
$T = 50 \text{ K}$						
Calc. (Ω_{DFT})	20.03	25.73	5.84	20.45	2.74	5.02
Expt.	65.73	68.31	35.89	7.18	3.31	0.94
$T = 300 \text{ K}$						
Calc. (Ω_{DFT})	3.42	4.89	0.56	2.48	0.66	0.38
Calc. ($\Omega_{295\text{K}}$)	0.96	2.24	0.20	0.61	0.29	0.19
Expt.	0.79	1.34	0.31	0.58	0.63	0.39

naphthalene, it is plausible that inclusion of electron-electron correlation has a significant effect on the renormalization; however, we defer this investigation to future work.

C. Electrical mobilities

We compute the electrical mobilities of the electrons (μ^e) and the holes (μ^h) in the self-energy relaxation-time approximation [40,77,78] with the expression

$$\mu_{\alpha}^{e,h}(T) = \frac{-e}{\rho_{e,h}\Omega} \sum_n \int \frac{d\mathbf{k}}{\Omega_{\text{BZ}}} \frac{\partial f(\varepsilon, T)}{\partial \varepsilon} \bigg|_{\varepsilon_{n\mathbf{k}}} |v_{n\mathbf{k},\alpha}|^2 \tau_{n\mathbf{k}}(T), \quad (9)$$

where α is the Cartesian direction of the applied electric field and the current, $\rho_{e,h}$ is the carrier density of the electrons or the holes, Ω and Ω_{BZ} are the volumes of the unit cell and the Brillouin zone, $v_{n\mathbf{k},\alpha}$ is the velocity of the electronic state $n\mathbf{k}$ along direction α , and the sum over bands is restricted to conduction bands for μ^e and valence bands for μ^h . The lifetimes $\tau_{n\mathbf{k}}$ are obtained from the imaginary part of the electron-phonon self-energy

$$\tau_{n\mathbf{k}}^{-1}(T) = \frac{2}{\hbar} \text{Im}[\Sigma_{n\mathbf{k}}^{\text{ep}}(\varepsilon_{n\mathbf{k}}^0, T)]. \quad (10)$$

To evaluate Eq. (9), we use the WANNIER90 package [79] to interpolate our computed electronic eigenvalues and velocities to a $60 \times 60 \times 60$ \mathbf{k} -grid. Calculating the EPC on this fine mesh is prohibitively expensive. We find, however, that the frequency-dependent self-energy for the bands around the gap is nearly independent of \mathbf{k} for naphthalene (see the Supplemental Material for a detailed analysis [42]). We therefore obtain the lifetimes $\tau_{n\mathbf{k}}$ on the dense \mathbf{k} -grid by interpolating the self-energy $\Sigma_{n\mathbf{k}'}^{\text{ep}}$ of a single point \mathbf{k}' using the approximation

$$\tau_{n\mathbf{k}}^{-1}(T) \approx \frac{2}{\hbar} \text{Im}[\Sigma_{n\mathbf{k}'}^{\text{ep}}(\varepsilon_{n\mathbf{k}}^0, T)]. \quad (11)$$

To minimize errors associated with this approximation, we choose \mathbf{k}' to be at A for the hole and Γ for the electron mobility, the locations of the VBM and CBM, respectively.

The calculated temperature-dependent hole and electron mobilities are shown in Table I for the directions a , b , and c^* (cf. Fig. 1). We compare the mobilities at 50 and 300 K,

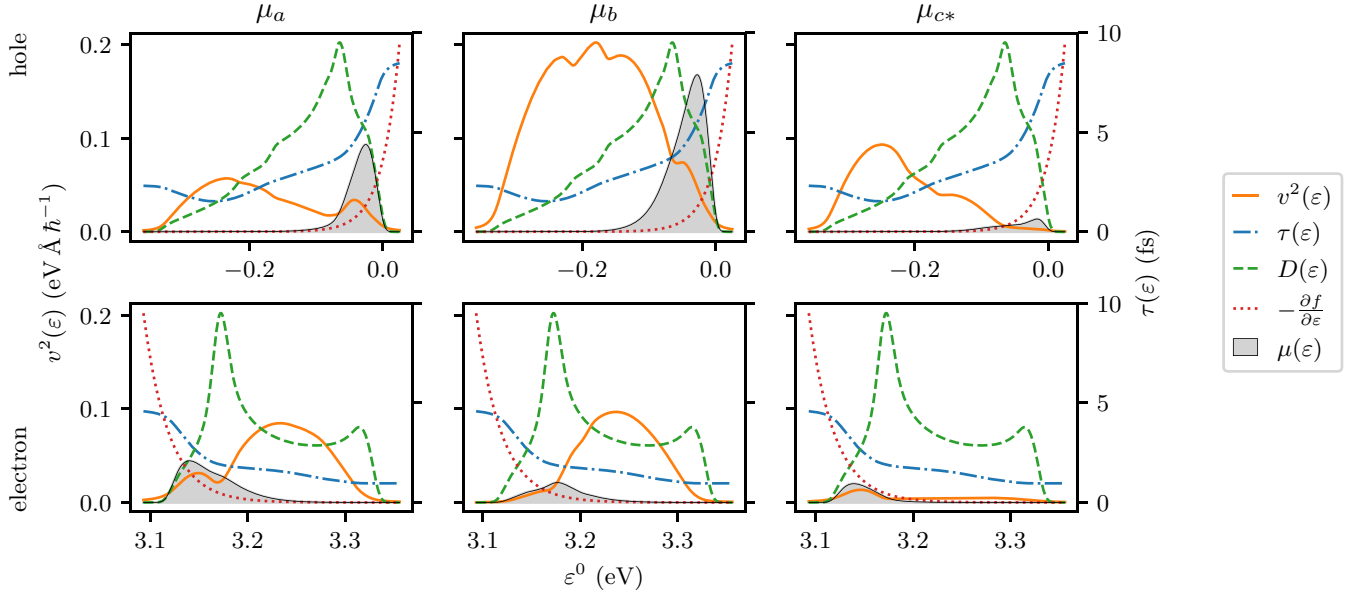


FIG. 5. The energy-resolved decomposition of the mobility according to Eq. (12) of holes (top) and electrons (bottom) at 300 K and the experimental room-temperature structure with Ω_{295K} . The velocity (orange solid) and the lifetime (blue dash-dot) are associated with the left and right y-axes, respectively. The density of states $D(\varepsilon)$ (green dashed), the derivative of the Fermi-Dirac distribution (red dotted), and the mobility integrand (gray filled) are in arbitrary units, but share the same scale across all plots.

using the relaxed (Ω_{DFT}) and experimental room-temperature volume (Ω_{295K}), respectively. Below 50 K, the mobilities become dependent on the electric field. At the same time, the volume between 5 and 50 K expands less than 0.5%, and the contribution of thermal lattice expansion to the mobility at these temperatures is expected to still be negligible. This allows us to use the relaxed lattice parameters and to extract the contribution of the lattice expansion to the mobility.

At 50 K, our calculations generally underestimate the hole mobilities, consistent with prior work [25], and overestimate the electron mobilities. At 300 K, the agreement with experiment is reasonably good when using the experimental lattice parameters. This suggests that electronic band transport limited by phonon scattering accounts for much of the electrical mobility. It is also apparent that the lattice expansion plays an important role in obtaining accurate values, as the agreement at 300 K greatly improves in most cases when using the room-temperature unit cell with Ω_{295K} . To more accurately predict the power law (or the slope) of the experimental mobilities, calculations need to be repeated using experimental lattice parameters obtained at different temperatures. This has been shown to lead to good agreement of the power law exponents in prior work [25]. Possible reasons for any disagreement with experiment include our neglect of polaronic effects and the physics of a hopping transport mechanism. In particular, at temperatures above 100 K, the experimental electron mobilities in the b and c^* direction show a decreased temperature dependence, commonly attributed to the transition to hopping transport [6,81–83] (see also the Supplemental Material [42]). Nonetheless, our work can be considered an important baseline for comparing with experiments and future work incorporating polaronic effects.

To gain insight into the mobilities, we decompose them into energy-resolved contributions by approximating Eq. (9)

in the following way:

$$\mu_{\alpha}^{e,h} \approx \frac{-e}{\rho_{e,h}} \int d\varepsilon D(\varepsilon) f'(\varepsilon) v_{\alpha}^2(\varepsilon) \tau(\varepsilon), \quad (12)$$

where $D(\varepsilon)$ is the density of states (DOS), $f'(\varepsilon)$ is the derivative of the Fermi-Dirac distribution with respect to energy, and where we define the average squared velocity function

$$v_{\alpha}^2(\varepsilon) = \frac{1}{D(\varepsilon)} \sum_n \int \frac{d\mathbf{k}}{\Omega_{BZ}} (v_{n\mathbf{k},\alpha})^2 \delta(\varepsilon - \varepsilon_{n\mathbf{k}}), \quad (13)$$

and the average lifetime function

$$\tau(\varepsilon) = \frac{1}{D(\varepsilon)} \sum_n \int \frac{d\mathbf{k}}{\Omega_{BZ}} \tau_{n\mathbf{k}} \delta(\varepsilon - \varepsilon_{n\mathbf{k}}). \quad (14)$$

The bounds of the integral in Eq. (12) go from $-\infty$ to the Fermi energy ε_F for holes, and from ε_F to $+\infty$ for electrons, and we add a small Gaussian smearing of 5 meV to evaluate the Dirac δ functions in Eq. (13) and (14).

Equation (12) approximates the energy-resolved contributions to the mobilities as the product of four functions of energy. We plot these quantities for Ω_{295K} in Fig. 5. At 300 K, the contributions to the mobilities extend up to about 0.1 eV above or below the band edges. Within this region, the DOS, velocity, and lifetime are generally not monotonic functions of energy, but show distinct features. This highlights the need for our detailed calculations; in contrast, for example, approximations of the mobility that only use the effective mass of the band extrema or constant effective lifetimes will be inadequate. This is especially true for μ_b^e , where the main contribution to the mobility is situated near the peak of the DOS, almost 0.1 eV within the conduction band. Using this analysis, we can also explain why the electron mobilities are generally lower than the hole mobilities.

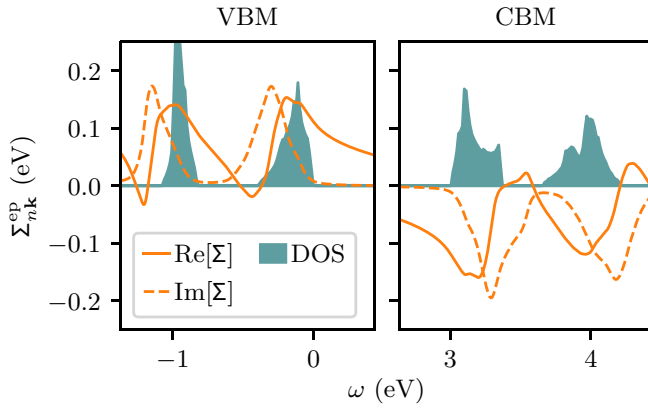


FIG. 6. The real (solid) and imaginary part (dashed) of the electron-phonon self-energy of naphthalene, evaluated for the VBM at A (left) and CBM at Γ (right). The features of the self-energy correlate with the electronic DOS (filled).

Comparing the individual quantities, we see that the velocities of electrons along the a and c^* directions are actually larger than those of the holes. However, the lower electron lifetimes compared to the hole lifetimes, especially near the band edge, more than compensate for the higher velocities. In general, this analysis shows the critical role the individual contributions of Eq. (9) play in quantitatively determining the mobility.

While the expression in Eq. (12) is of great practicality for computing the mobilities and visualizing the energy-resolved lifetimes and velocities, it also turns out to be an excellent approximation. The maximum relative error compared to Eq. (9) is below 10%, and the mean absolute relative error is below 5%. Mobilities calculated with this approximation deviate less than 3.3% (see the Supplemental Material [42]). In addition to being independent of \mathbf{k} , the frequency-dependent self-energies of the two highest (lowest) valence (conduction) bands are almost identical. This is because the wave functions, and hence the electron-phonon matrix elements, of Davydov pairs are so similar for naphthalene (see [42]). Within this \mathbf{k} - and n -independent approximation, the electron and hole lifetimes are only a function of energy, and the expressions in Eqs. (9) and (12) become equivalent.

D. Self-consistent electron-phonon self-energy

Figure 6 shows the frequency-dependent electron-phonon self-energy of the valence- and conduction-band extrema alongside the electronic DOS. We see a clear correlation. This is mainly due to the fact that the electron-phonon coupling matrix elements are relatively independent of \mathbf{k} and n within a Davydov pair. The imaginary part of Eq. (2) then becomes proportional to the joint electronic and vibrational density of states, weighted by the coupling strength of each phonon. In agreement with previous studies [25,37], we find that intramolecular modes around 0.19 eV have the strongest coupling (Fig. 4). Correspondingly, the peaks of the SE are shifted by about 0.19 eV compared to the peaks of the DOS.

We also note from Fig. 6 that the real part of the electron-phonon self-energy varies rapidly between 0 and 0.15 eV over

the frequency range corresponding to the bandwidth, which is on the order of 0.4 eV. The renormalization of the bands will therefore significantly alter the shape and width of the DOS, upon which the self-energy depends. The magnitude of the self-energy corrections suggests that we should compute the self-energy self-consistently by updating the electronic energies in Eq. (2) with the renormalized values.

Accordingly, we use an eigenvalue–self-consistent (evSC) cycle for the self-energy, whose iterative steps can be summarized as

$$\begin{aligned}\varepsilon_{n\mathbf{k}}^1 &= \varepsilon_{n\mathbf{k}}^0 + \text{Re}[\Sigma_{n\mathbf{k}}^{\text{ep}}(\varepsilon_{n\mathbf{k}}^0, \varepsilon_{m\mathbf{k}+\mathbf{q}}^0)], \\ \varepsilon_{n\mathbf{k}}^2 &= \varepsilon_{n\mathbf{k}}^0 + \text{Re}[\Sigma_{n\mathbf{k}}^{\text{ep}}(\varepsilon_{n\mathbf{k}}^1, \varepsilon_{m\mathbf{k}+\mathbf{q}}^1)], \\ &\dots \\ \varepsilon_{n\mathbf{k}}^i &= \varepsilon_{n\mathbf{k}}^0 + \text{Re}[\Sigma_{n\mathbf{k}}^{\text{ep}}(\varepsilon_{n\mathbf{k}}^{i-1}, \varepsilon_{m\mathbf{k}+\mathbf{q}}^{i-1})],\end{aligned}\quad (15)$$

where $\Sigma_{n\mathbf{k}}^{\text{ep}}(\varepsilon_{n\mathbf{k}}^{i-1}, \varepsilon_{m\mathbf{k}+\mathbf{q}}^{i-1})$ indicates the use of renormalized eigenvalues in the self-energy. We use the \mathbf{k} -independence approximation to efficiently calculate the renormalized states $m\mathbf{k} + \mathbf{q}$ as

$$\varepsilon_{m\mathbf{k}+\mathbf{q}}^i \approx \varepsilon_{m\mathbf{k}+\mathbf{q}}^0 + \text{Re}[\Sigma_{n\mathbf{k}}^{\text{ep}}(\varepsilon_{m\mathbf{k}+\mathbf{q}}^{i-1})]. \quad (16)$$

This procedure converges the renormalized energies rapidly to within 2 meV for the bands around the gap (see the Supplemental Material [42]).

Our method effectively includes all high-order noncrossing electron-phonon coupling diagrams in the self-energy. It does not, however, allow for multiphonon satellite bands to form in the spectral function, as, for example, the cumulant expansion would [84]. A similar level of theory to evSC was previously achieved using a time propagation of the Green's function [85].

While the self-consistent calculation of the electron-phonon coupling self-energy offers a clear description of the quasiparticle temperature renormalization and lifetimes, one generally aims to compute these quantities from a one-shot calculation of the self-energy for practical reasons. Two different procedures are often used. In the on-the-mass-shell approximation [72], which we have used so far, the renormalized energies are computed according to Eq. (7). A more rigorous approach, in theory, is to evaluate the self-energy at the quasiparticle energy, corresponding to the peak of the

TABLE II. Comparison of the one-shot self-energy computed in the on-the-mass-shell approximation [$\Sigma(\varepsilon^0)$], the one-shot self-energy evaluated at the quasiparticle solution [$\Sigma(\varepsilon)$], and the eigenvalue–self-consistent self-energy (evSC). Renormalizations $\Delta\varepsilon$ are in eV, lifetimes τ in fs.

	$\Sigma(\varepsilon^0)$	$\Sigma(\varepsilon)$	evSC
$\Delta\varepsilon_{\text{VBM}} (0 \text{ K})$	0.11	0.09	0.12
$\Delta\varepsilon_{\text{CBM}} (0 \text{ K})$	−0.12	−0.09	−0.12
$\tau_{\text{VBM}} (300 \text{ K})$	8.70	38.47	7.91
$\tau_{\text{CBM}} (300 \text{ K})$	4.73	21.16	6.42

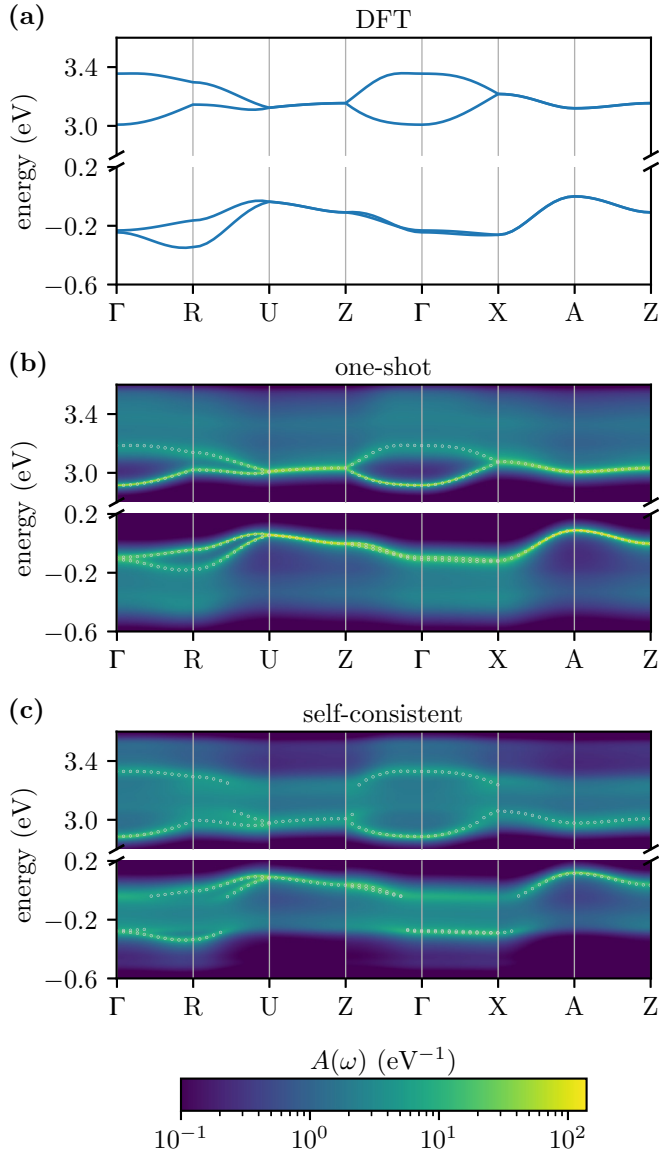


FIG. 7. (a) The DFT-PBE-D3 band structure of naphthalene of the two highest valence and two lowest conduction bands. (b) and (c) The spectral function of the full band structure calculated using the (b) one-shot and (c) self-consistent method. To highlight the renormalized band structure, the highest peak for each state $n\mathbf{k}$, i.e., the solution to Eq. (17) with the smallest imaginary part, is marked with a dot. While the one-shot spectral function displays a continuous quasiparticle band structure, the self-consistent result shows discontinuities.

spectral function, that is,

$$\varepsilon_{n\mathbf{k}}(T) = \varepsilon_{n\mathbf{k}}^0 + \text{Re}[\Sigma_{n\mathbf{k}}^{\text{ep}}(\varepsilon_{n\mathbf{k}}, T)]. \quad (17)$$

In Table II, we compare the two one-shot procedures against the self-consistent scheme. For the VBM and the CBM, the on-the-mass-shell approximation appears to better reproduce the self-consistent scheme, both for the real and imaginary parts of the self-energy. The quasiparticle solution vastly overestimates the lifetimes of the band extrema (see the Supplemental Material [42]). For the real part of the self-energy,

TABLE III. Mobilities calculated at 300 K with experimental lattice parameters ($\Omega_{295\text{K}}$), using the one-shot and self-consistent (evSC) method, in comparison with experimental values. All values in $\text{cm}^2/\text{V s}$.

	Hole			Electron		
	μ_a	μ_b	μ_{c^*}	μ_a	μ_b	μ_{c^*}
one-shot	1.20	2.73	0.24	0.67	0.31	0.21
evSC	0.90	2.19	0.18	1.18	0.59	0.31
Expt.	0.79	1.34	0.31	0.58	0.63	0.39

such a result agrees with the one found for the Fröhlich model, compared with diagrammatic Monte Carlo results [84,86].

Next, we examine the effect of the evSC approach through the spectral function, given by the imaginary part of the Green's function:

$$A_{n\mathbf{k}}(\omega) = \frac{1}{\pi} \frac{|\text{Im}[\Sigma_{n\mathbf{k}}^{\text{ep}}(\omega)]|}{[\omega - \varepsilon_{n\mathbf{k}}^0 - \text{Re}[\Sigma_{n\mathbf{k}}^{\text{ep}}(\omega)]^2 + \text{Im}[\Sigma_{n\mathbf{k}}^{\text{ep}}(\omega)]^2}. \quad (18)$$

It describes the probability of finding an electron in state $n\mathbf{k}$ at energy ω . The quasiparticle (QP) peaks of the spectral function appear at $\omega = \varepsilon_{n\mathbf{k}}^0 - \text{Re}[\Sigma_{n\mathbf{k}}^{\text{ep}}(\omega)]$, which corresponds to the solution of Eq. (17). The spectral function allows us to compare both the renormalization (position of the QP peak) and the broadening (width and height of the QP peak) simultaneously.

Figure 7 shows both the one-shot and evSC spectral function, where we use the \mathbf{k} -independence approximation to interpolate $A_{n\mathbf{k}}(\omega)$ across the Brillouin zone. We chose the self-energy at Γ as a starting point for the interpolation, and we checked that the choice of starting point does not alter the results significantly.

The QP bands of the evSC spectral function show a discontinuity at energies around 0.2 eV below the VBM and above the CBM, due to the spectral weight being transferred from the main quasiparticle peak to the satellite band. In contrast, the bands of the one-shot calculation are continuous, and the distinction between the main quasiparticle peak and the satellite remains clear in most cases. This band discontinuity (or splitting) happens when the real part of the self-energy has a unitless slope $\gtrsim 1$. In this case, the Dyson equation (17) may admit more than one solution in certain regions of the Brillouin zone. Such a high slope in the self-energy is seen near the poles, located one phonon frequency away from the peaks of the DOS, as seen in Fig. 6 (the strongest coupling modes are ~ 0.19 eV). A similar splitting has also been observed theoretically and experimentally in pentacene and rubrene crystals [35,36,87] as well as nonorganic systems [50,88].

Finally, we evaluate the mobilities from the evSC self-energy at 300 K using $\Omega_{295\text{K}}$ lattice parameters, taking into account the renormalized electronic eigenvalues and velocities. The results are listed in Table III in comparison with the values for the one-shot calculation and experiment. The evSC approach lowers the hole mobilities, bringing μ_a and μ_b to even better agreement with experiment. In contrast,

evSC electron mobilities increase slightly compared to the one-shot calculation. By looking at the decomposition of the mobility via Eq. (12), we can attribute the decrease of the hole mobility to lower lifetimes, and the increase of the electron mobilities to higher lifetimes and velocities (see the Supplemental Material [42] for the decomposition).

III. CONCLUSION

In summary, we used comprehensive *ab initio* calculations based on DFT to study the effect of electron-phonon interactions on the electronic structure of naphthalene crystals, as well as its electrical mobility. Both the temperature-dependent renormalization of the gap, and the hole and electron mobilities are in good agreement with experimental values if the lattice expansion is taken into account. Because of the limited dependence of the self-energy on \mathbf{k} and n of the two occupied and unoccupied band-edge bands, we can visualize the contributions to the mobility at each band energy in terms of the density of states, average scattering time, and average velocity squared. This facilitates a useful energy-resolved analysis of the mobility, and provides an efficient way to model charge carrier transport in organic systems.

Furthermore, we indirectly and approximately investigated the effect of higher-order electron-phonon coupling terms by calculating the self-energy self-consistently. The band gap renormalization and mobilities show only moderate differences between the one-shot and self-consistent calculations, as long as the on-the-mass-shell approximation is used. Both of these properties depend mainly on the electronic states close to the band gap, which are only weakly affected by the evSC treatment. However, the electronic states further

away from the band edges are strongly affected by the self-consistent treatment of the self-energy. The spectral function reveals a band splitting and band widening comparable to what has been observed experimentally in other molecular crystals.

Most of the qualitative results discussed in this work result directly from the weak interactions between constituent monomers, a common feature of molecular crystals. This includes the \mathbf{k} -independence of the self-energy, and the band-widths being on the same order of magnitude as the phonon frequencies.

The methods and conclusions presented here likely apply to several other molecular crystals, and they provide an efficient approach for the *ab initio* calculation of the electron-phonon self-energy and electrical mobility.

ACKNOWLEDGMENTS

This work was supported by the Theory FWP at the Lawrence Berkeley National Laboratory, which is funded by the US Department of Energy (DOE), Office of Science, Basic Energy Sciences, Materials Sciences and Engineering Division under Contract No. DE-AC0205CH11231, and by the Fonds de la Recherche Scientifique (F.R.S.-FNRS Belgium) through the PdR Grants No. T.0238.13 - AIXPHO (X.G., M.G.) and No. T.0103.19 - ALPS (X.G., M.G.). Computational resources were provided by the National Energy Research Scientific Computing Center, which is supported by the Office of Science. C.D. acknowledges support by the Deutsche Forschungsgemeinschaft (DFG) - Projektnummer 182087777 - SFB 951.

-
- [1] O. D. Jurchescu, J. Baas, and T. T. M. Palstra, Effect of impurities on the mobility of single crystal pentacene, *Appl. Phys. Lett.* **84**, 3061 (2004).
 - [2] J. Takeya, M. Yamagishi, Y. Tominari, R. Hirahara, Y. Nakazawa, T. Nishikawa, T. Kawase, T. Shimoda, and S. Ogawa, Very high-mobility organic single-crystal transistors with in-crystal conduction channels, *Appl. Phys. Lett.* **90**, 102120 (2007).
 - [3] H. Minemawari, T. Yamada, H. Matsui, J. Tsutsumi, S. Haas, R. Chiba, R. Kumai, and T. Hasegawa, Inkjet printing of single-crystal films, *Nature (London)* **475**, 364 (2011).
 - [4] S. Fratini, S. Ciuchi, D. Mayou, G. T. de Laissardière, and A. Troisi, A map of high-mobility molecular semiconductors, *Nat. Mater.* **16**, 998 (2017).
 - [5] V. A. Dediu, L. E. Hueso, I. Bergenti, and C. Taliani, Spin routes in organic semiconductors, *Nat. Mater.* **8**, 707 (2009).
 - [6] F. Ortmann, F. Bechstedt, and K. Hannewald, Charge transport in organic crystals: Interplay of band transport, hopping and electron-phonon scattering, *New J. Phys.* **12**, 023011 (2010).
 - [7] X. Gao and Z. Zhao, High mobility organic semiconductors for field-effect transistors, *Sci. China Chem.* **58**, 947 (2015).
 - [8] C. Wang, H. Dong, L. Jiang, and W. Hu, Organic semiconductor crystals, *Chem. Soc. Rev.* **47**, 422 (2018).
 - [9] K. Hannewald, V. M. Stojanović, J. M. T. Schellekens, P. A. Bobbert, G. Kresse, and J. Hafner, Theory of polaron bandwidth narrowing in organic molecular crystals, *Phys. Rev. B* **69**, 075211 (2004).
 - [10] M. Pope and C. E. Swenberg, *Electronic Processes in Organic Crystals and Polymers*, 2nd ed. (Oxford University Press, New York, 1999).
 - [11] F. Ortmann, F. Bechstedt, and K. Hannewald, Charge transport in organic crystals: Theory and modelling, *Phys. Status Solidi B* **248**, 511 (2011).
 - [12] O. Ostroverkhova, Organic optoelectronic materials: Mechanisms and applications, *Chem. Rev.* **116**, 13279 (2016).
 - [13] M. Ohtomo, T. Suzuki, T. Shimada, and T. Hasegawa, Band dispersion of quasi-single crystal thin film phase pentacene monolayer studied by angle-resolved photoelectron spectroscopy, *Appl. Phys. Lett.* **95**, 123308 (2009).
 - [14] R. C. Hatch, D. L. Huber, and H. Höchst, Electron-Phonon Coupling in Crystalline Pentacene Films, *Phys. Rev. Lett.* **104**, 047601 (2010).

- [15] K. Hannewald and P. A. Bobbert, *Ab initio* theory of charge-carrier conduction in ultrapure organic crystals, *Appl. Phys. Lett.* **85**, 1535 (2004).
- [16] A. Troisi, D. L. Cheung, and D. Andrienko, Charge Transport in Semiconductors with Multiscale Conformational Dynamics, *Phys. Rev. Lett.* **102**, 116602 (2009).
- [17] A. Girlando, L. Grisanti, M. Masino, I. Bilotti, A. Brillante, R. G. Della Valle, and E. Venuti, Peierls and Holstein carrier-phonon coupling in crystalline rubrene, *Phys. Rev. B* **82**, 035208 (2010).
- [18] J. E. Northrup, Two-dimensional deformation potential model of mobility in small molecule organic semiconductors, *Appl. Phys. Lett.* **99**, 062111 (2011).
- [19] M. Casula, M. Calandra, and F. Mauri, Local and nonlocal electron-phonon couplings in K_3 picene and the effect of metallic screening, *Phys. Rev. B* **86**, 075445 (2012).
- [20] J. Xi, M. Long, L. Tang, D. Wang, and Z. Shuai, First-principles prediction of charge mobility in carbon and organic nanomaterials, *Nanoscale* **4**, 4348 (2012).
- [21] H. Kobayashi, N. Kobayashi, S. Hosoi, N. Koshitani, D. Murakami, R. Shirasawa, Y. Kudo, D. Hobara, Y. Tokita, and M. Itabashi, Hopping and band mobilities of pentacene, rubrene, and 2,7-diocetyl[1]benzothieno[3,2-b][1]benzothiophene (C8-BTBT) from first principle calculations, *J. Chem. Phys.* **139**, 014707 (2013).
- [22] A. Heck, J. J. Kranz, T. Kubař, and M. Elstner, Multi-scale approach to non-adiabatic charge transport in high-mobility organic semiconductors, *J. Chem. Theory Comput.* **11**, 5068 (2015).
- [23] H. Ishii, N. Kobayashi, and K. Hirose, Charge transport calculations by a wave-packet dynamical approach using maximally localized Wannier functions based on density functional theory: Application to high-mobility organic semiconductors, *Phys. Rev. B* **95**, 035433 (2017).
- [24] H. Oberhofer, K. Reuter, and J. Blumberger, Charge transport in molecular materials: An assessment of computational methods, *Chem. Rev.* **117**, 10319 (2017).
- [25] N.-E. Lee, J.-J. Zhou, L. A. Agapito, and M. Bernardi, Charge transport in organic molecular semiconductors from first principles: The bandlike hole mobility in a naphthalene crystal, *Phys. Rev. B* **97**, 115203 (2018).
- [26] V. Stehr, R. F. Fink, C. Deibel, and B. Engels, Charge carrier mobilities in organic semiconductor crystals based on the spectral overlap, *J. Comput. Chem.* **37**, 2146 (2016).
- [27] H. Ishii, J.-i. Inoue, N. Kobayashi, and K. Hirose, Quantitative mobility evaluation of organic semiconductors using quantum dynamics based on density functional theory, *Phys. Rev. B* **98**, 235422 (2018).
- [28] A. Marini, *Ab Initio* Finite-Temperature Excitons, *Phys. Rev. Lett.* **101**, 106405 (2008).
- [29] F. Giustino, S. G. Louie, and M. L. Cohen, Electron-Phonon Renormalization of the Direct Band Gap of Diamond, *Phys. Rev. Lett.* **105**, 265501 (2010).
- [30] H. Kawai, K. Yamashita, E. Cannuccia, and A. Marini, Electron-electron and electron-phonon correlation effects on the finite-temperature electronic and optical properties of zinc-blende gan, *Phys. Rev. B* **89**, 085202 (2014).
- [31] S. Ponc  , Y. Gillet, J. Laflamme Janssen, A. Marini, M. Verstraete, and X. Gonze, Temperature dependence of the electronic structure of semiconductors and insulators, *J. Chem. Phys.* **143**, 102813 (2015).
- [32] J. P. Nery and P. B. Allen, Influence of Fr  hlich polaron coupling on renormalized electron bands in polar semiconductors: Results for zinc-blende GaN, *Phys. Rev. B* **94**, 115135 (2016).
- [33] G. Antonius, S. Ponc  , P. Boulanger, M. C    , and X. Gonze, Many-Body Effects on the Zero-Point Renormalization of the Band Structure, *Phys. Rev. Lett.* **112**, 215501 (2014).
- [34] B. Monserrat, E. A. Engel, and R. J. Needs, Giant electron-phonon interactions in molecular crystals and the importance of nonquadratic coupling, *Phys. Rev. B* **92**, 140302(R) (2015).
- [35] S. Ciuchi, R. C. Hatch, H. H  chst, C. Faber, X. Blase, and S. Fratini, Molecular Fingerprints in the Electronic Properties of Crystalline Organic Semiconductors: From Experiment to Theory, *Phys. Rev. Lett.* **108**, 256401 (2012).
- [36] F. Bussolotti, J. Yang, T. Yamaguchi, K. Yonezawa, K. Sato, M. Matsunami, K. Tanaka, Y. Nakayama, H. Ishii, N. Ueno, and S. Kera, Hole-phonon coupling effect on the band dispersion of organic molecular semiconductors, *Nat. Commun.* **8**, 173 (2017).
- [37] N. Vukmirovi  , C. Bruder, and V. M. Stojanovi  , Electron-Phonon Coupling in Crystalline Organic Semiconductors: Microscopic Evidence for Nonpolaronic Charge Carriers, *Phys. Rev. Lett.* **109**, 126407 (2012).
- [38] S. Ponc  , G. Antonius, Y. Gillet, P. Boulanger, J. Laflamme Janssen, A. Marini, M. C    , and X. Gonze, Temperature dependence of electronic eigenenergies in the adiabatic harmonic approximation, *Phys. Rev. B* **90**, 214304 (2014).
- [39] A. Marini, S. Ponc  , and X. Gonze, Many-body perturbation theory approach to the electron-phonon interaction with density-functional theory as a starting point, *Phys. Rev. B* **91**, 224310 (2015).
- [40] F. Giustino, Electron-phonon interactions from first principles, *Rev. Mod. Phys.* **89**, 015003 (2017).
- [41] G. Antonius, S. Ponc  , E. Lantagne-Hurtubise, G. Auclair, X. Gonze, and M. C    , Dynamical and anharmonic effects on the electron-phonon coupling and the zero-point renormalization of the electronic structure, *Phys. Rev. B* **92**, 085137 (2015).
- [42] See Supplemental Material at <http://link.aps.org/supplemental/10.1103/PhysRevB.101.165102> for lattice parameters, full phonon dispersion, convergence studies, justification for the \mathbf{k} -independence approximation of the self-energy, temperature dependence of electrical mobilities and evaluation of the mobility decomposition, and detailed analysis of the effect of evSC on the self-energy and spectral function.
- [43] P. B. Allen and V. Heine, Theory of the temperature dependence of electronic band structures, *J. Phys. C* **9**, 2305 (1976).
- [44] X. Gonze, P. Boulanger, and M. C    , Theoretical approaches to the temperature and zero-point motion effects on the electronic band structure, *Ann. Phys.* **523**, 168 (2011).
- [45] A. Eiguen and C. Ambrosch-Draxl, Wannier interpolation scheme for phonon-induced potentials: Application to bulk MgB_2 , W, and the 1×1 H-covered W(110) surface, *Phys. Rev. B* **78**, 045124 (2008).
- [46] C. Verdi and F. Giustino, Fr  hlich Electron-Phonon Vertex from First Principles, *Phys. Rev. Lett.* **115**, 176401 (2015).
- [47] X. Gonze, B. Amadon, G. Antonius, F. Arnardi, L. Baguet, J.-M. Beuken, B. Bieder, F. Bottin, J. Bouchet, E. Bousquet, N. Brouwer, F. Bruneval, G. Brunin, T. Cavignac, J.-B. Charraud, W. Chen, M. C    , S. Cottenier, J. Denier, G. Geneste, P.

- Ghosez, M. Giantomassi, Y. Gillet, O. Gingras, D. R. Hamann, G. Hautier, X. He, N. Helbig, N. Holzwarth, Y. Jia, F. Jollet, W. Lafargue-Dit-Hauret, K. Lejaeghere, M. A. Marques, A. Martin, C. Martins, H. P. Miranda, F. Naccarato, K. Persson, G. Petretto, V. Planes, Y. Pouillon, S. Prokhorenko, F. Ricci, G.-M. Rignanese, A. H. Romero, M. M. Schmitt, M. Torrent, M. J. van Setten, B. V. Troeye, M. J. Verstraete, G. Zerah, and J. W. Zwanziger, The abinit project: Impact, environment and recent developments, *Comput. Phys. Commun.* **248**, 107042 (2020).
- [48] J. Sjakste, N. Vast, M. Calandra, and F. Mauri, Wannier interpolation of the electron-phonon matrix elements in polar semiconductors: Polar-optical coupling in GaAs, *Phys. Rev. B* **92**, 054307 (2015).
- [49] F. Giustino, M. L. Cohen, and S. G. Louie, Electron-phonon interaction using Wannier functions, *Phys. Rev. B* **76**, 165108 (2007).
- [50] A. Eiguren and C. Ambrosch-Draxl, Complex Quasiparticle Band Structure Induced by Electron-Phonon Interaction: Band Splitting in the 1×1 H/W(110) Surface, *Phys. Rev. Lett.* **101**, 036402 (2008).
- [51] X. Gonze, B. Amadon, P. Anglade, J. Beuken, F. Bottin, P. Boulanger, F. Bruneval, D. Caliste, R. Caracas, M. Côté, T. Deutsch, L. Genovese, P. Ghosez, M. Giantomassi, S. Goedecker, D. R. Hamann, P. Hermet, F. Jollet, G. Jomard, S. Leroux, M. Mancini, S. Mazevet, M. J. T. Oliveira, G. Onida, Y. Pouillon, T. Rangel, G.-M. Rignanese, D. Sangalli, R. Shaltaf, M. Torrent, M. J. Verstraete, G. Zerah, and J. W. Zwanziger, ABINIT: First-principles approach to material and nanosystem properties, *Comput. Phys. Commun.* **180**, 2582 (2009).
- [52] X. Gonze, F. Jollet, F. A. Araujo, D. Adams, B. Amadon, T. Applencourt, C. Audouze, J.-M. Beuken, J. Bieder, A. Bokhanchuk, E. Bousquet, F. Bruneval, D. Caliste, M. Côté, F. Dahm, F. D. Pieve, M. Delaveau, M. D. Gennaro, B. Dorado, C. Espejo, G. Geneste, L. Genovese, A. Gerossier, M. Giantomassi, Y. Gillet, D. Hamann, L. He, G. Jomard, J. L. Janssen, S. L. Roux, A. Levitt, A. Lherbier, F. Liu, I. Lukačević, A. Martin, C. Martins, M. Oliveira, S. Poncé, Y. Pouillon, T. Rangel, G.-M. Rignanese, A. Romero, B. Rousseau, O. Rubel, A. Shukri, M. Stankovski, M. Torrent, M. Van Setten, B. Van Troeye, M. Verstraete, D. Waroquiers, J. Wiktor, B. Xue, A. Zhou, and J. Zwanziger, Recent developments in the abinit software package, *Comput. Phys. Commun.* **205**, 106 (2016).
- [53] M. Fuchs and M. Scheffler, *Ab initio* pseudopotentials for electronic structure calculations of poly-atomic systems using density-functional theory, *Comput. Phys. Commun.* **119**, 67 (1999).
- [54] S. Grimme, J. Antony, S. Ehrlich, and H. Krieg, A consistent and accurate *ab initio* parametrization of density functional dispersion correction (DFT-D) for the 94 elements H-Pu, *J. Chem. Phys.* **132**, 154104 (2010).
- [55] S. Grimme, S. Ehrlich, and L. Goerigk, Effect of the damping function in dispersion corrected density functional theory, *J. Comput. Chem.* **32**, 1456 (2011).
- [56] X. Gonze and C. Lee, Dynamical matrices, Born effective charges, dielectric permittivity tensors, and interatomic force constants from density-functional perturbation theory, *Phys. Rev. B* **55**, 10355 (1997).
- [57] S. Baroni, S. de Gironcoli, A. Dal Corso, and P. Giannozzi, Phonons and related crystal properties from density-functional perturbation theory, *Rev. Mod. Phys.* **73**, 515 (2001).
- [58] X. Gonze, G. M. Rignanese, and R. Caracas, First-principle studies of the lattice dynamics of crystals, and related properties, *Z. Kristallogr.* **220**, 458 (2005).
- [59] B. Van Troeye, M. Torrent, and X. Gonze, Interatomic force constants including the DFT-D dispersion contribution, *Phys. Rev. B* **93**, 144304 (2016).
- [60] F. Brown-Altvater, T. Rangel, and J. B. Neaton, *Ab initio* phonon dispersion in crystalline naphthalene using van der Waals density functionals, *Phys. Rev. B* **93**, 195206 (2016).
- [61] T. Rangel, K. Berland, S. Sharifzadeh, F. Brown-Altvater, K. Lee, P. Hyldgaard, L. Kronik, and J. B. Neaton, Structural and excited-state properties of oligoacene crystals from first principles, *Phys. Rev. B* **93**, 115206 (2016).
- [62] I. R. Thomas, I. J. Bruno, J. C. Cole, C. F. Macrae, E. Pidcock, and P. a. Wood, WebCSD: the online portal to the Cambridge Structural Database, *J. Appl. Crystallogr.* **43**, 362 (2010); Cambridge Structural Database <http://webofsd.ccdc.cam.ac.uk/>.
- [63] S. C. Capelli, A. Albinati, S. a. Mason, and B. T. M. Willis, Molecular motion in crystalline naphthalene: Analysis of multi-temperature X-ray and neutron diffraction data, *J. Phys. Chem. A* **110**, 11695 (2006).
- [64] A. S. Davydov, The theory of molecular excitons, *Sov. Phys. Usp.* **7**, 145 (1964).
- [65] E. F. Sheka, Davydov splitting in the absorption spectra of molecular crystals, *Mol. Cryst. Liq. Cryst.* **29**, 323 (1975).
- [66] I. Natkaniec, E. L. Bokhenkov, B. Dorner, J. Kalus, G. A. Mackenzie, G. S. Pawley, U. Schmelzer, and E. F. Sheka, Phonon dispersion in d₈-naphthalene crystal at 6 K, *J. Phys. C* **13**, 4265 (1980).
- [67] M. Suzuki, T. Yokoyama, and M. Ito, Polarized Raman spectra of naphthalene and anthracene single crystals, *Spectrochim. Acta Part Mol. Spectrosc.* **24**, 1091 (1968).
- [68] A. Troisi and G. Orlandi, Charge-Transport Regime of Crystalline Organic Semiconductors: Diffusion Limited by Thermal Off-Diagonal Electronic Disorder, *Phys. Rev. Lett.* **96**, 086601 (2006).
- [69] V. Coropceanu, R. S. Sánchez-Carrera, P. Paramonov, G. M. Day, and J.-L. Brédas, Interaction of charge carriers with lattice vibrations in organic molecular semiconductors: Naphthalene as a case study, *J. Phys. Chem. C* **113**, 4679 (2009).
- [70] L. Wang and D. Beljonne, Flexible surface hopping approach to model the crossover from hopping to band-like transport in organic crystals, *J. Phys. Chem. Lett.* **4**, 1888 (2013).
- [71] X. Xie, A. Santana-Bonilla, and A. Troisi, Nonlocal electron-phonon coupling in prototypical molecular semiconductors from first principles, *J. Chem. Theory Comput.* **14**, 3752 (2018).
- [72] E. Cannuccia and A. Marini, Zero point motion effect on the electronic properties of diamond, trans-polyacetylene and polyethylene, *Eur. Phys. J. B* **85**, 320 (2012).
- [73] C. L. Braun and G. M. Dobbs, Intrinsic photoconductivity in naphthalene single crystals, *J. Chem. Phys.* **53**, 2718 (1970).
- [74] C. Faber, I. Duchemin, T. Deutsch, C. Attaccalite, V. Olevano, and X. Blase, Electron-phonon coupling and charge-transfer excitations in organic systems from many-body perturbation theory: The Fiesta code, an efficient Gaussian-basis

- implementation of the *GW* and Bethe-Salpeter formalisms, *J. Mater. Sci.* **47**, 7472 (2012).
- [75] B. Monserrat, Correlation effects on electron-phonon coupling in semiconductors: Many-body theory along thermal lines, *Phys. Rev. B* **93**, 100301(R) (2016).
- [76] Z. Li, G. Antonius, M. Wu, F. H. da Jornada, and S. G. Louie, Electron-Phonon Coupling from *Ab Initio* Linear-Response Theory Within the *GW* Method: Correlation-Enhanced Interactions and Superconductivity in $\text{Ba}_{1-x}\text{K}_x\text{BiO}_3$, *Phys. Rev. Lett.* **122**, 186402 (2019).
- [77] M. Bernardi, D. Vigil-Fowler, J. Lischner, J. B. Neaton, and S. G. Louie, *Ab Initio* Study of Hot Carriers in the First Picosecond After Sunlight Absorption in Silicon, *Phys. Rev. Lett.* **112**, 257402 (2014).
- [78] S. Ponc , E. R. Margine, and F. Giustino, Towards predictive many-body calculations of phonon-limited carrier mobilities in semiconductors, *Phys. Rev. B* **97**, 121201(R) (2018).
- [79] A. A. Mostofi, J. R. Yates, G. Pizzi, Y.-S. Lee, I. Souza, D. Vanderbilt, and N. Marzari, An updated version of WANNIER90: A tool for obtaining maximally-localised Wannier functions, *Comput. Phys. Commun.* **185**, 2309 (2014).
- [80] *Ternary Compounds, Organic Semiconductors*, edited by O. Madelung, U. R ssler, and M. Schulz, Landolt-B rnstein-Group III, Condensed Matter, Vol. 41E (Springer-Verlag, Berlin/Heidelberg, 2000).
- [81] L. B. Schein, C. B. Duke, and A. R. McGhie, Observation of the Band-Hopping Transition for Electrons in Naphthalene, *Phys. Rev. Lett.* **40**, 197 (1978).
- [82] L. B. Schein and A. R. McGhie, Band-hopping mobility transition in naphthalene and deuterated naphthalene, *Phys. Rev. B* **20**, 1631 (1979).
- [83] W. Warta and N. Karl, Hot holes in naphthalene: High, electric-field-dependent mobilities, *Phys. Rev. B* **32**, 1172 (1985).
- [84] J. P. Nery, P. B. Allen, G. Antonius, L. Reining, A. Miglio, and X. Gonze, Quasiparticles and phonon satellites in spectral functions of semiconductors and insulators: Cumulants applied to the full first-principles theory and the Fr hlich polaron, *Phys. Rev. B* **97**, 115145 (2018).
- [85] D. Dunn, Electron-phonon interactions in an insulator, *Can. J. Phys.* **53**, 321 (1975).
- [86] A. S. Mishchenko, N. V. Prokof'ev, A. Sakamoto, and B. V. Svistunov, Diagrammatic quantum Monte Carlo study of the Fr hlich polaron, *Phys. Rev. B* **62**, 6317 (2000).
- [87] S. Ciuchi and S. Fratini, Band Dispersion and Electronic Lifetimes in Crystalline Organic Semiconductors, *Phys. Rev. Lett.* **106**, 166403 (2011).
- [88] A. Eiguren, C. Ambrosch-Draxl, and P. M. Echenique, Self-consistently renormalized quasiparticles under the electron-phonon interaction, *Phys. Rev. B* **79**, 245103 (2009).